Biochimica et Biophysica Acta 1788 (2009) 1869–1876

Contents lists available at ScienceDirect

Biochimica et Biophysica Acta

journal homepage: www.elsevier.com/locate/bbamem

The effect of salt and pH on block liposomes studied by cryogenic transmission electron microscopy

Alexandra Zidovska [a], Kai K. Ewert [a], Joel Quispe [b], Bridget Carragher [b], Clinton S. Potter [b], Cyrus R. Safinya [a,*]

[a] Materials, Physics, and Molecular, Cellular and Developmental Biology Departments, University of California at Santa Barbara, Santa Barbara, CA 93106, USA
[b] National Resource for Automated Molecular Microscopy, Department of Cell Biology, The Scripps Research Institute, 10550 North Torrey Pines Road, La Jolla, CA 92037, USA

ARTICLE INFO

Article history:
Received 20 February 2009
Received in revised form 12 June 2009
Accepted 15 June 2009
Available online 23 June 2009

Keywords:
Block liposome
Charged membrane
Curvature stabilization
Cryo-TEM

ABSTRACT

Recently, we have reported the discovery of block liposomes (BLs), a new class of liquid (chain-melted) vesicles, formed in mixtures of the curvature-stabilizing hexadecavalent cationic lipid MVLBG2, the neutral lipid 1,2-dioleoyl-*sn*-glycero-3-phosphatidylcholine (DOPC), and water with no added salt. BLs consist of connected spheres, pears, tubes, or rods. Unlike in typical liposome systems, where spherical vesicles, tubular vesicles, and cylindrical micelles are separated on the macroscopic scale, shapes remain connected and are separated only on the nanometer scale within a single BL. Here, we report structural studies of the effect of salt and pH on the BL phase, carried out using differential interference contrast microscopy (DIC) and cryogenic transmission electron microscopy (cryo-TEM). Addition of salt screens the electrostatic interactions; in low-salt conditions, partial screening of electrostatic interactions leads to a shape transition from BLs to bilamellar vesicles, while in the high-salt regime, a shape transition from BLs to liposomes with spherical morphologies occurs. This demonstrates that strong electrostatic interactions are essential for BL formation. Understanding the control of liposome shape evolution is of high interest because such shape changes play an important role in many intracellular processes such as endocytosis, endoplasmatic reticulum-associated vesiculation, vesicle recycling and signaling.

1. Introduction

Lipid molecules play a key role in cell biology. Their amphiphilic nature dictates them to assemble into lipid bilayers in an aqueous environment, which is of crucial importance for cellular function. Lipid bilayers, also called membranes, define the boundaries of a cell and within a cell (compartmentalization); they facilitate intracellular trafficking and thus aid macromolecular transport and signal transduction; and they enable endo- as well as exocytosis [1]. Membranes also serve as an embedding matrix for many proteins, enabling their proper function. For many of the membrane functions and processes mentioned above, membrane shape evolution is critical. The majority of membrane shapes found in cells are known to be caused by an interplay of proteins and lipids [2–4]. There are several different established mechanisms leading to membrane deformation in cells: (i) curvature-stabilizing proteins like clathrin, caveolin or BAR domains generate membrane curvature by attaching to the membrane surface and building an exoskeleton (scaffold); (ii) certain integral membrane proteins possess an intrinsic curvature or generate curvature upon oligomerization (e.g., K^+-channel, nicotinic acetylcholine receptor); (iii) cytoskeletal activity can cause membrane remodeling, enabling cell motility (actin filaments, microtubules); (iv) an amphiphatic α-helix can be actively inserted into the lipid bilayer to generate curvature (e.g., epsin, endophilin); (v) motor proteins can generate tubules (e.g., dynamin); and (vi) a change in lipid composition involving a lipid of nonzero intrinsic curvature can also lead to change in membrane curvature [5–10]. In the present work, we have focused on the latter mechanism, investigating the influence of lipid molecular shape and charge on the membrane shape evolution.

Recently, we have reported the discovery of block liposomes (BLs) in a model *in vitro* system. BLs are a new vesicle phase resulting from membrane shape evolution upon the addition of a membrane curvature-forming and -stabilizing lipid, MVLBG2, to bilayers of DOPC [11]. BLs are formed in mixtures of MVLBG2, DOPC and water at specific compositions (8–10 mol% MVLBG2). They consist of distinctly shaped, nanoscale spheres, pears, tubes, or rods which remain connected. Cryo-TEM has identified diblocks (pear–tube) and triblocks (pear–tube–pear) consisting of nanoscale tubules (cylindrical vesicles) connected to spherical vesicles as well as

Abbreviations: BLs, block liposomes; CL, cationic lipid; cryo-TEM, cryo transmission electron microscopy; DIC, differential interference contrast microscopy; DOPC, 1,2-dioleoyl-*sn*-glycero-3-phosphatidylcholine

* Corresponding author. Materials Department, University of California at Santa Barbara, Santa Barbara, CA 93106, USA.
E-mail address: safinya@mrl.ucsb.edu (C.R. Safinya).

0005-2736/$ – see front matter © 2009 Elsevier B.V. All rights reserved.
doi:10.1016/j.bbamem.2009.06.013

diblocks (sphere–rod) consisting of rods (cylindrical micelles) connected to spherical vesicles. Fig. 1A shows BLs containing nanotube regions, with nanotubes highlighted by white arrows. The diameter of the nanotubes may vary from 10 to 50 nm. Fig. 1B shows a rare pentablock BL, consisting of five blocks: sphere–tube–sphere–tube–sphere, with nanotube regions highlighted by white arrows. Fig. 1C shows a diblock BL consisting of a spherical vesicle and a cylindrical micelle (rod). The micellar region is highlighted by two pairs of arrowheads at different locations along the rod. The diameter of the cylindrical micelle equals the thickness of the bilayer ($\approx$4 nm). Of note, not a single instance of a free cylindrical micelle is present in the samples.

A model of the BL formation has been proposed previously where thermal, compositional and/or counterion concentration fluctuations were suggested as different pathways leading to the lateral curvature-induced lipid phase separation within a BL [11]. The structure of the BLs implies a phase separation of the lipid components within the membrane due to the fact that a block liposome is a single object consisting of two or more regions (sphere and tube, or sphere and rod) of drastically different membrane spontaneous curvature C_0 while the membrane bending rigidity $\kappa \gg k_B T$.

Fig. 2A shows molecular models of DOPC and MVLBG2. MVLBG2 is a newly synthesized, highly charged (16+) lipid with a dendritic headgroup. Its headgroup area is several times larger than that of neutral, zwitterionic DOPC while the tails of the two molecules are essentially identical [12]. This high charge and conical molecular shape of MVLBG2 generate a high spontaneous curvature when MVLBG2 is incorporated into a lipid monolayer. Consequently, mixtures of MVLBG2 and DOPC, which has a cylindrical molecular shape, exhibit a rich phase diagram with novel vesicle morphologies. Fig. 2B shows schematic drawings of DOPC (white) and MVLBG2 (green) based on the molecular models shown in Fig. 2A. Fig. 2C schematically depicts a triblock (sphere–tube–sphere), with the two insets showing the proposed molecular arrangement within the marked areas. A breaking of symmetry in the composition between the outer and inner monolayer of the tubular region facilitates high curvature. Schematics of a diblock (sphere–rod) are depicted in Fig. 2D. The two insets are enlarged views, illustrating the proposed molecular arrangements for the rod region as well as the attachment of the rod (cylindrical micelle) to the spherical vesicle.

In this work, we report investigations on the effect of salt and pH on BLs, employing cryo-TEM to characterize their nanoscale

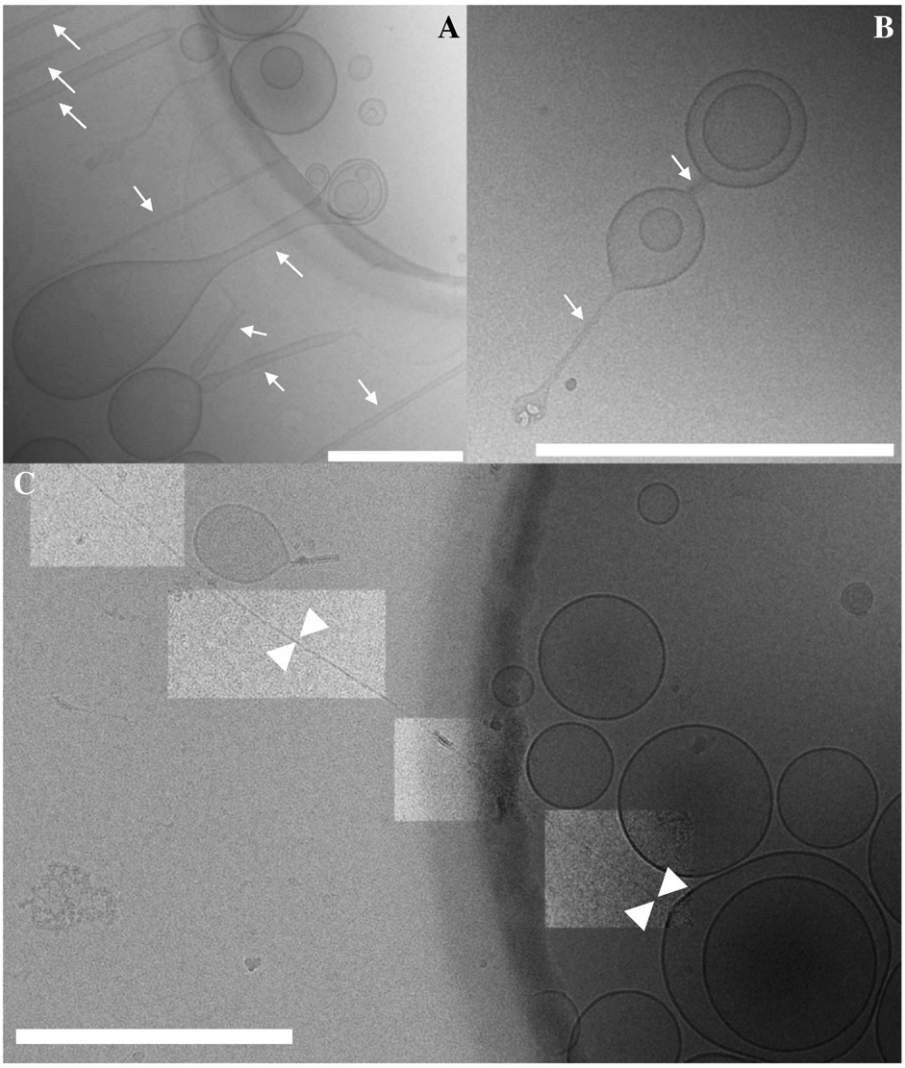

Fig. 1. Cryo-TEM of block liposomes (BLs). (A, B) Cryo-TEM images of BLs formed in mixtures of MVLBG2, DOPC and water. BLs consist of distinctly shaped nanoscale blocks – spheres, pears, tubes, or rods – which remain connected. White arrows are pointing to nanotube regions of the BLs. (C) Cryo-TEM image of a diblock (sphere–rod). The rod segment (cylindrical micelle attached to the vesicle) is highlighted with two pairs of white arrowheads. Scale bar, 500 nm.

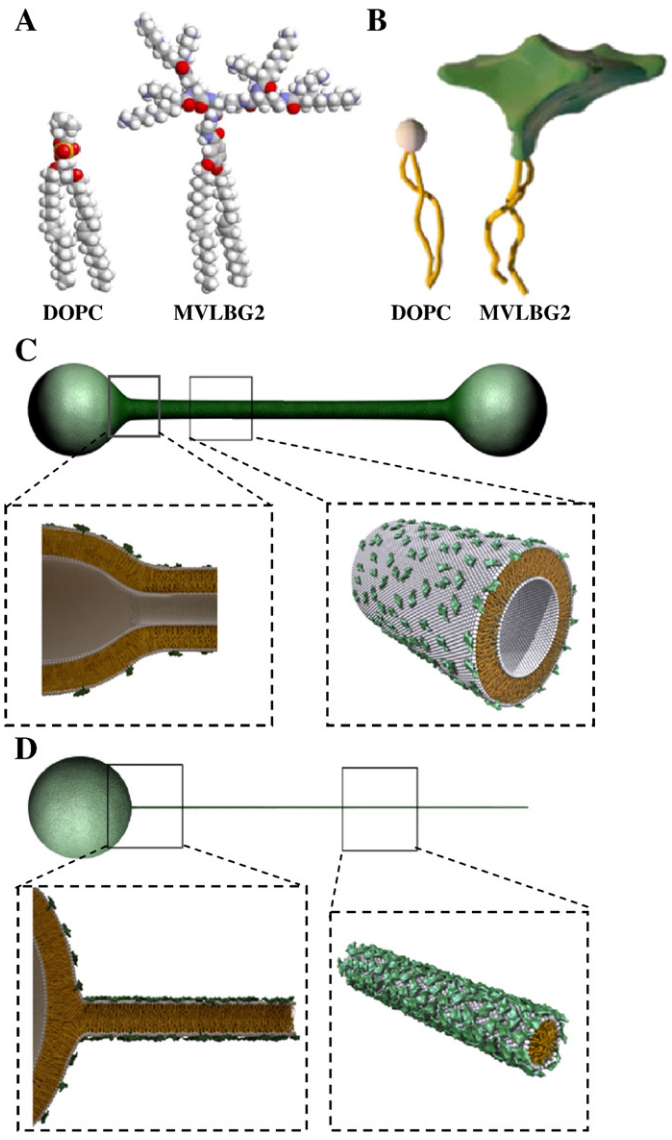

Fig. 2. Schematics of block liposomes. (A) Molecular models of neutral DOPC and hexadecavalent MVLBG2. (B) Schematics of DOPC and MVLBG2 based on the models shown in part A. (C) Schematic of a triblock (sphere–tube–sphere). The insets depict the proposed molecular arrangement for the regions marked by rectangular boxes. Note the breaking of compositional symmetry in the tubular region. (D) Schematic of a diblock (sphere–rod). The insets depict the proposed molecular arrangement for the regions marked by rectangular boxes. Note the topological transition from bilayer (of the spherical vesicle) to cylindrical micelle (left inset) at this unique connection.

structures. The addition of salt causes screening of the charge of MVLBG2 and forces BLs to undergo shape transitions to other morphologies. These depend on the extent of the electrostatic screening, given by the salt concentration in the system. BLs transform into bilamellar vesicles at 50 mM salt and multilamellar vesicles at 250 mM salt. This effect of salt on the shape evolution of the BLs demonstrates the key role of electrostatic interactions in the system. We further carried out structural studies of the BL-forming lipid mixture under different pH conditions. The change in pH of the solution changes the protonation of MVLBG2, altering the charge as well as the size of its headgroup. The resulting change in the molecular shape of MVLBG2 affects the spontaneous curvature C_0 of MVLBG2-containing lipid monolayers, potentially enabling reversible control of shape transitions. However, all pH buffers are also salts, and the effect of salt was dominant for the ready-made pH buffers used in our experiments.

2. Materials and methods

2.1. Materials

DOPC was purchased as a solution in chloroform from Avanti Polar Lipids. MVLBG2 was synthesized as described [12]. NaCl stock solutions were prepared in deionized water at final concentrations of 50 mM, 100 mM, 250 mM and 500 mM. Ready-made buffer solutions at pH 4 (BX1628-1; 1.02 wt.% Potassium Hydrogen Phthalate, 0.02 wt.% HCl, 0.003 wt.% Amaranth, 0.05 wt.% sodium o-phenylphenate (Dowicide A), >98 wt.% water) and pH 10 (BX1641-1; <1.00 wt.% Na_2CO_3, <1.00 wt.% $NaHCO_3$, <1.00 wt.% Patient Blue A, 0.05 wt.% 1-(3-chloroallyl)-3,5,7-triaza-1-azonia-adamantane chloride (Dowicil 75), >97 wt.% water) were purchased from EMD Chemicals.

2.2. Lipid solutions

Solutions of MVLBG2 trifluoroacetate were prepared in chloroform/methanol (9:1, v/v). Lipid solutions were combined at the desired ratio of lipids and dried, first by a stream of nitrogen and subsequently in a vacuum for 8–24 h. High resistivity (18.2 MΩ cm) water was added to the residue, and the mixture was incubated at 37 °C for at least 12 h to give a final concentration of 10 mg/mL. If applicable, the aqueous lipid solutions were mixed (1:1, v/v) with the salt solutions and pH buffers, respectively, giving a final lipid concentration of 5 mg/mL and a final salt/buffer concentration of half the original salt/buffer concentration. All concentration values given in the text refer to these final concentrations. The samples were allowed to equilibrate for 24 h at room temperature, then stored at 4 °C until use. Another way of preparation, where the dried lipids were rehydrated with the salt/buffer solutions of final concentration, then incubated at 37 °C for at least 12 h to give a final lipid concentration of 5 mg/mL, and stored at 4 °C until use, gave the same results as observed with DIC microscopy. The pH of MVLBG2/DOPC aqueous lipid solutions was measured using indicator paper (due to the small sample volume) as 5.5 ± 0.5, which corresponds to an average MVLBG2 charge of $+14.5$ e to $+16$ e.

2.3. Optical Microscopy

A Nikon Diaphot 300 inverted microscope equipped for epifluorescence and DIC and a SensiCamQE high-speed digital camera were used.

2.4. Cryo-TEM

The specimens were preserved in a layer of vitreous ice suspended over a holey carbon substrate. The holey carbon films consist of a thin layer of pure carbon fenestrated by 2 μm holes spaced 4 μm apart and suspended over 400 mesh copper grids [13]. The grids were cleaned prior to vitrification with a Solarus plasma cleaner (Gatan Inc.) using a 25% O_2 and 75% Ar mixture. Samples were vitrified by plunge freezing into liquid ethane using a Vitrobot (FEI Co.). The vitrified sample was then imaged using a Tecnai F20 (FEI Co.) electron microscope at 120 keV. Images were collected using a 4096×4096 pixel CCD camera (TVPIS GmbH) at the search magnification of 5000 and final magnifications of 29000 to 280000 at an underfocus of ~2.5 μm. The Leginon software system [14] was used for data collection, data storage as well as partial data analysis. The analysis of the intralamellar distances was performed on the original, high resolution images collected on the microscope (4096×4096 pixels) using Adobe Photoshop software. The images displayed in the figures are of lower resolution than these original images.

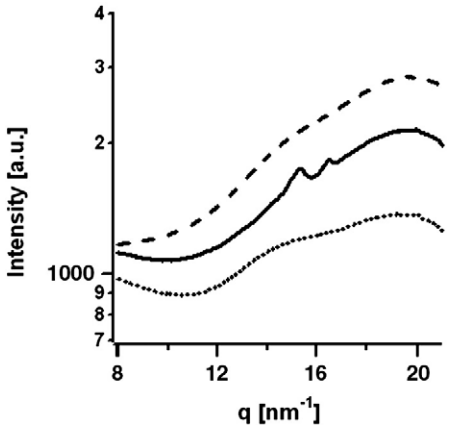

Fig. 3. BL membrane phase determination via WAXS. Typical signatures representing the liquid-disordered (dotted line, DOPS/DOPC, 50/50, mol/mol) and liquid-ordered states of membranes (solid line, DSPS/DSPC/cholesterol, 50/40/10, mol/mol/mol). The WAXS data for MVLBG2/DOPC (dashed line, 10/90, mol/mol) show a broad lipid peak at $q \approx 14\ \mathrm{nm}^{-1}$, indicating disordered lipid chains in the membrane. This is in contrast to all previously reported lipid nanotubes which are in the liquid-ordered phase.

2.5. Wide-angle X-ray scattering

Lipid solutions of final lipid concentration of 10 mg/mL were placed into 1.5 mm quartz capillaries and flame sealed. Wide-angle X-ray scattering data was collected on an in-house setup consisting of a rotating copper anode source operated by a Rigaku RU-300 generator. The wavelength of radiation (Cu K_α) was 1.54 Å. A set of Confocal Max Flux Optics (Osmics, Inc.) was used to focus the beam. A Mar CCD image plate detector of 345 mm diameter was used (Mar USA, Evanston, IL). Silver behenate was used as the calibration standard. Data collection was performed for 2 h (no radiation damage occurred in the sample during this time). The acquired X-ray scattering data were integrated over 360° to obtain plots of scattering intensity versus momentum transfer.

3. Results and discussion

3.1. Block liposome membranes are in the fluid phase

Wide-angle X-ray scattering (WAXS) proved that the membranes comprising BLs are in the fluid (liquid-disordered) phase. Fig. 3 summarizes the typical WAXS signatures of the liquid-disordered, L_α, and the liquid-ordered, L_β, states of a membrane (obtained from 1,2-dioleoyl-*sn*-glycero-3-phosphatidyl-serine (DOPS)/DOPC, 50/50, mol/mol, dotted line, and 1,2-distearoyl-*sn*-glycero-3-phosphatidyl-serine (DSPS)/1,2-distearoyl-*sn*-glycero-3-phosphatidylcholine (DSPC)/cholesterol, 50/40/10, mol/mol/mol, solid line, respectively). BLs show a broad peak at $q \approx 14\ \mathrm{nm}^{-1}$, indicating a disordered lipid phase (dashed line), in striking contrast to all previously reported lipid nanotubes which are in the liquid-ordered phase. This is a potential advantage for applications, such as the incorporation of functional biomolecules, which typically require the membrane to be in the fluid (chain-melted) state to retain their full biological activity, and could lead to bioactive "liquid" nanotubes for a range of applications including sensing and chemical delivery.

3.2. The effect of salt on block liposomes

The effect of salt on the MVLBG2/DOPC/water system is documented in Figs. 4 and 5. The addition of salt screens the electrostatic interactions, which may be quantified by the Debye screening length (κ^{-1}): $\kappa^{-1} = (\varepsilon_0 \varepsilon k_B T / 1000 N_A e^2 \Sigma c_i Z_i^2)^{1/2}$ [15]. We have studied two different regimes: low (50 mM NaCl) and high (250 mM NaCl) salt concentrations, for which the Debye screening length is 1.359 nm and 0.608 nm, respectively (Table 1). The effect of salt on block liposomes was investigated employing differential interference contrast microscopy (DIC) and cryo-TEM. The combination of these two microscopy techniques allows studying the system on the micrometer as well as the nanometer scale.

DIC microscopy (Fig. 4) shows that in the low-salt regime, BLs aggregate at their spherical caps (Fig. 4A–D) with the cylindrical parts

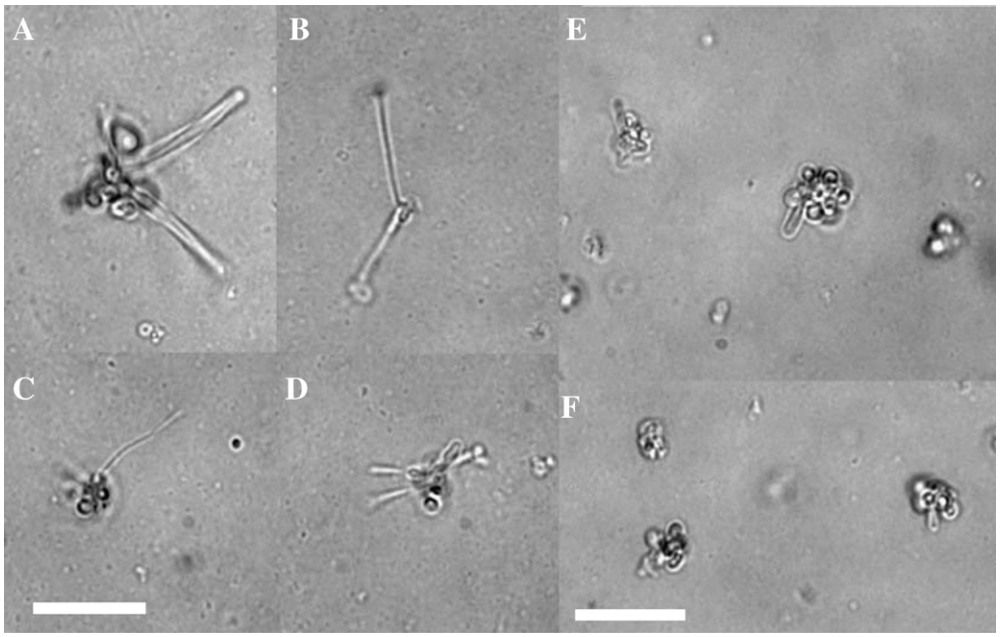

Fig. 4. The effect of salt on the BL-forming MVLBG2/DOPC lipid mixture on the micrometer scale. DIC images of a mixture of MVLBG2 and DOPC (10/90, mol/mol) in salt solution: (A–D) 50 mM NaCl and (E, F) 250 mM NaCl. The total lipid concentration in all samples is 5 mg/mL. The Debye length is 1.36 nm and 0.61 nm for 50 mM and 250 mM NaCl, respectively. Scale bars, 10 μm.

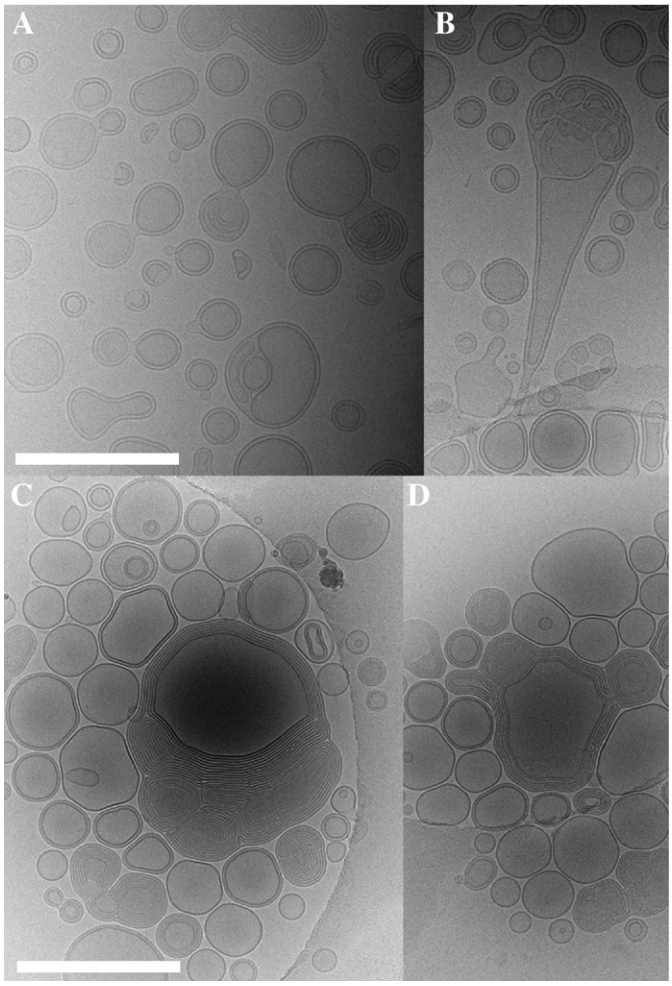

Fig. 5. The effect of salt on the BL-forming MVLBG2/DOPC lipid mixture on the nanometer scale. Cryo-TEM images of a mixture of MVLBG2 and DOPC (10/90, mol/mol) in salt solution: (A, B) 50 mM NaCl and (C, D) 250 mM NaCl. The total lipid concentration in all samples is 5 mg/mL. The Debye length is 1.36 nm and 0.61 nm for 50 mM and 250 mM NaCl, respectively. Scale bars, 500 nm.

pointing outwards. Upon further addition of salt, the phase behavior of the system changes radically. In the high-salt regime DIC microscopy shows aggregates reminiscent of the aggregated spherical parts of the BLs under low-salt conditions but lacking the cylindrical extensions (Fig. 4E and F).

In the low-salt regime, cryo-TEM reveals that unlike on the micrometer scale, there are no BL aggregates present on the nanometer scale. Instead, primarily bilamellar vesicles are found as shown in Fig. 5A and B. The inner lumen of these vesicles consists of one, two or more vesicles. An abundant morphology are dumbbell-shaped vesicles, where the spherical parts of the outer vesicle each contain another, smaller spherical vesicle. The outer bilayer wraps tightly around the inner vesicles at a constant intralamellar distance (Fig. 5A) of 4–6 nm. It is instructive to compare these structures to sphere–tube–sphere BLs, from which they can be derived by contracting the tubular block into the short neck of the dumbbell vesicles. Of note, most BLs observed in water (Figs. 1) also contain spherical vesicles within their spherical blocks, albeit without a well-defined intralamellar distance. Fig. 5B displays an example of an elongated vesicle with a rather pronounced tubular region with varying diameter which is another characteristic morphology found in the low-salt regime. These structures are again filled with internal vesicles, leading mostly to bilamellar vesicles. The striking common feature for all morphologies seen in the low-salt regime is the presence of two lamellae. No BLs were found under these conditions.

In the high-salt regime, cryo-TEM images reveal the presence of unilamellar, bilamellar and multilamellar structures with a constant intralamellar distance of ≈4 nm, persisting over tens of lamellae. Fig. 5C and D shows examples of such multilamellar vesicles. As depicted in Fig. 5C, the organization of the lamellae within the multilamellar structures can be complex, with several multilamellar vesicles tightly packed inside a larger one. However, the intralamellar distance remains unchanged. As in the low-salt regime, no BLs were found.

In order to understand the shape transitions which the BL-forming MVLBG2/DOPC lipid mixture undergoes in the presence of salt, one has to consider that a membrane's spontaneous curvature is given by the molecular shapes of the incorporated lipids. The effective molecular shape of a charged or a zwitterionic lipid, however, is defined not only by the sterical arrangement of the atoms (including their hydration radius), but also by the electrostatic interaction between the charges residing on the molecule. Therefore, the effective spontaneous curvature of a monolayer consisting of such a lipid molecule is $C_0^{\mathrm{eff}} = C_0^{\mathrm{steric}} + C_0^{\mathrm{electrostatic}}$. The higher the charge of the lipid molecule, the larger the contribution of $C_0^{\mathrm{electrostatic}}$. In the presence of salt, $C_0^{\mathrm{electrostatic}}$ is reduced due to the electrostatic screening, leading to an overall decrease in C_0^{eff}. In addition, the presence of salt screens the electrostatic interaction between the charged lipid bilayers.

For the MVLBG2/DOPC system in the low-salt regime, $C_0^{\mathrm{electrostatic}}$ has been significantly reduced, favoring vesicle morphologies with nearly zero curvature (spherical vesicles) and occasional tubular structures of large diameters. The pH of the solution slightly increases upon salt addition as judged by a side-by-side comparison of the color of a pH indicator paper. Since the only acidic component in the solution is MVLBG2, this corresponds to a decreased dissociation of protons from the MVLBG2 headgroup, implying an increased charge. This may be rationalized by a reduced intramolecular repulsion of the positive charges in the headgroup due to the salt in solution. Just as the electrostatic repulsion within the membrane, the repulsion between positively charged MVLBG2/DOPC membranes has also been screened to the extent of the Debye length of 1.359 nm. The observed bilamellar structures with a constant lamellar distance result from the competition between Van der Waals attraction and repulsive forces, which include hydration, electrostatic and undulation forces. Evidently, the screening of the electrostatic repulsion in the low-salt regime is sufficient to allow two bilayers to come close together, but not to allow further stacking of membranes. The shapes of the vesicles, e.g. of the dumbbells, indicate that the attraction between the membranes is quite strong, overcoming their bending rigidity. A transition from unilamellar to bilamellar vesicles has previously been observed only in a system consisting of a mixture of cationic and anionic surfactants upon addition of an amphiphatic biopolymer [16], where the mechanism proposed for this transition is the networking of the bilayers by the biopolymer.

In the high-salt regime, $C_0^{\mathrm{electrostatic}}$ is reduced further, resulting in the exclusive formation of membranes with zero spontaneous curvature. The pH of the solution slightly increases further (pH≈6), again implying a slightly increased charge of the MVLBG2 headgroup. The increased screening of the electrostatic repulsion between the membranes now allows the formation of multilamellar structures.

Table 1
Summary of the Debye lengths for different salt and buffer conditions, where $c_{1:1}$ and $c_{1:2}$ are the concentrations of 1:1 and 1:2 electrolytes in solution, respectively.

Salt/buffer	$c_{1:1}$ [mM]	$c_{1:2}$ [mM]	Debye length [nm]
Water	–	–	960
50 mM NaCl	50	–	1.36
250 mM NaCl	250	–	0.61
pH 4 buffer	60	–	1.24
pH 10 buffer	125	97	0.47

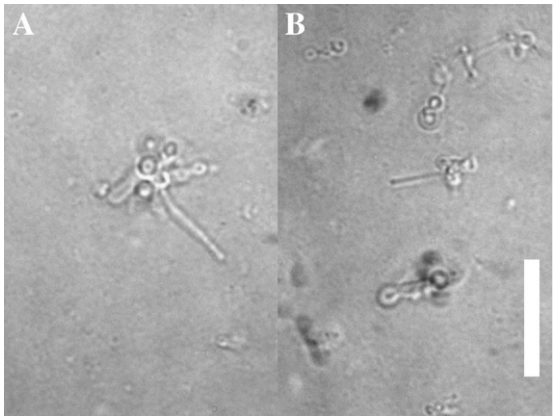

Fig. 6. The effect of buffer at pH = 4 on the BL-forming MVLBG2/DOPC lipid mixture on the micrometer scale. (A, B) DIC images of a mixture of MVLBG2 and DOPC (10/90, mol/mol) in buffer at pH = 4. The total lipid concentration is 5 mg/mL. Scale bar, 10 μm.

Again, the intralamellar spacing is given by the balance between Van der Waals attraction and the combined repulsive forces.

3.3. The effect of pH on block liposomes

The following section gives an overview of the impact of pH on the morphologies formed by the MVLBG2/DOPC lipid mixture. We varied the pH with the aim of controlling the membrane charge and curvature. The pH of the MVLBG2/DOPC lipid mixture in pure water was ~5.5, meaning that about one ammonium group per MVLBG2 trifluoroacetate molecule had transferred its proton to the aqueous medium. The headgroup of MVLBG2 contains four identical moieties which derive from the endogenous polyamine spermine. More than one set of pKa values for spermine can be found in the literature [17–20], but two are usually measured to be lower than 10, and all values lie between 11.5 and 7.9. Assuming that the pKa values of the spermine-like moieties in MVLBG2 are similar to those of spermine, MVLBG2 would essentially be fully protonated (in buffer) at pH<6.9 and partially protonated (less than 50%, i.e. 8+) at pH = 10. The changes in the protonation of the MVLBG2 headgroup are expected to not only modify the charge, but also the steric size of the headgroup due to changes in hydration and the intramolecular repulsion of charged moieties.

It is important to note that it is impossible to fully separate pH and salt effects because the buffers used to provide a constant pH are also salts. Table 1 summarizes the salt contents in the salt solutions and buffers used in our experiments and the corresponding Debye lengths. The buffer for pH = 10 contains both 1:1 electrolytes and 1:2 electrolytes. While this potentially complicates the interpretation of our data, due to valency-dependent effects, we have not observed effects of the divalent anions on the MVLBG2/DOPC lipid mixture beyond the increased electrostatic screening (which is considered in the calculation of the Debye length).

Figs. 6 and 7 provide an overview of the structures formed by the BL-forming MVLBG2/DOPC lipid mixture in a buffer solution of pH = 4 at both the micrometer and the nanometer scale. The DIC images shown in Fig. 6 demonstrate that under these conditions, block liposomes aggregate at their spherical caps, with their cylindrical segments pointing outwards. This behavior closely resembles the one observed in the low-salt regime.

Fig. 7 shows cryo-TEM images of the (BL-forming) MVLBG2/DOPC mixture in a buffer solution of pH = 4, which also reveal similarities with the low-salt regime (Fig. 5A and B): bilamellar vesicles (as seen under low-salt conditions) are abundant and bilamellar tubes are also present (Fig. 7A). As Fig. 7B demonstrates, the bilamellar structures consist of a lipid bilayer tightly wrapped around one, two or more internal vesicles. The Debye screening length in this solution is 1.24 nm, comparable to that in the low-salt regime (Table 1). In addition, as shown in Fig. 7A, BLs can occasionally be found under these conditions. In contrast to the BLs observed in pure water, the bending rigidity of the tubular regions is very low. Furthermore, no cylindrical micelles, whether free or attached to the vesicles, were found under these conditions. Fig. 7C shows an illustration of the changes in the MVLBG2 headgroup expected for pH = 4 in the presence of salt (here, 60 mM monovalent salt, cf. Table 1). The

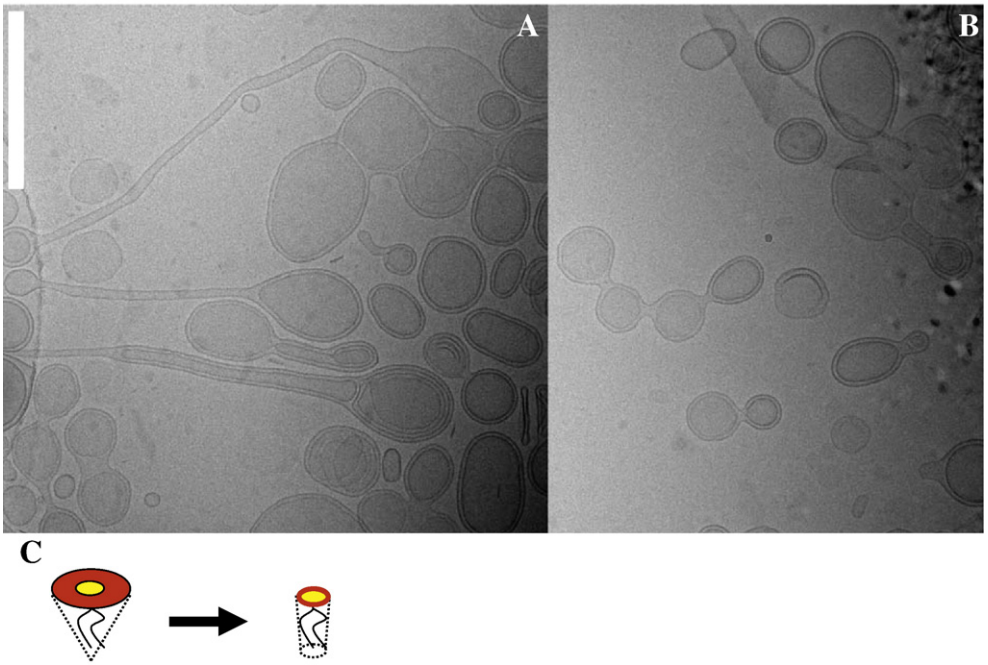

Fig. 7. The effect of buffer at pH = 4 on the BL-forming MVLBG2/DOPC lipid mixture on the nanometer scale. (A, B) Cryo-TEM images of a mixture of MVLBG2 and DOPC (10/90, mol/mol) in buffer at pH = 4. The total lipid concentration is 5 mg/mL. Scale bar, 500 nm. (C) A schematic visualizing the steric (yellow) and electrostatic (red) contributions to the size of the MVLBG2 headgroup and thus the lipid's molecular shape. The salt present in the buffer screens the electrostatic contribution (red), while the steric contribution (yellow) slightly increases at pH = 4 as the headgroup reaches full protonation.

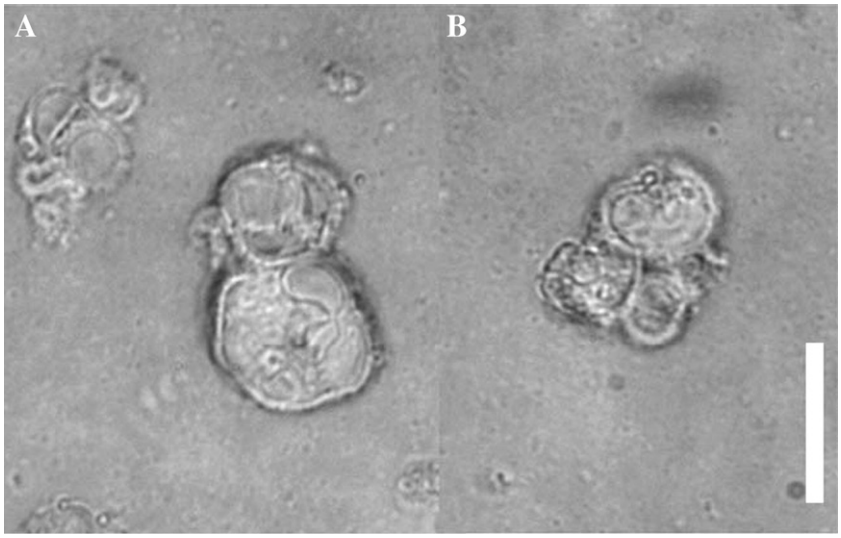

Fig. 8. The effect of buffer at pH = 10 on the BL-forming MVLBG2/DOPC lipid mixture on the micrometer scale. (A, B) DIC images of a mixture of MVLBG2 and DOPC (10/90, mol/mol) in buffer at pH = 10. The total lipid concentration is 5 mg/mL. Scale bar, 10 μm.

schematic visualizes the steric (yellow) and the electrostatic (red) contribution to the shape and size of the MVLBG2 headgroup. In the presence of salt, most of the electrostatic contribution (red) is screened, while the steric contribution (yellow) slightly increases at pH = 4 as the headgroup reaches full protonation. As observed in the low-salt regime, the buffer also partially screens the electrostatic repulsion of the charged membranes, allowing formation of bilamellar structures. However, the screening is not sufficient to permit stacking into multilamellar structures.

Figs. 8 and 9 show the BL-forming MVLBG2/DOPC lipid mixture in a buffer solution of pH = 10. Under these conditions, the MVLBG2/DOPC system readily transforms into large multilamellar vesicles as seen with DIC (Fig. 8A and B). As evident in Fig. 9A and B, cryo-TEM also shows large multilamellar vesicles. These structures are reminiscent of those seen under high-salt conditions, which may be expected because the Debye length is 0.47 nm, comparable to that of the high-salt regime (0.61 nm). The intralamellar spacing of 4–6 nm is however larger than the spacing under high-salt conditions and the number of lamellae is usually less than 10. Fig. 9C shows a schematic of the changes in the MVLBG2 headgroup expected for pH = 10. Again, the steric and electrostatic contributions are marked in yellow and red, respectively. The presence of salt screens the electrostatic contribution and the pH = 10 leads to at least a partial deprotonation of the headgroup, resulting in a reduction of its charge and steric size. The molecular shape thus changes from conical to cylindrical, corresponding to zero membrane spontaneous curvature (lamellar structures).

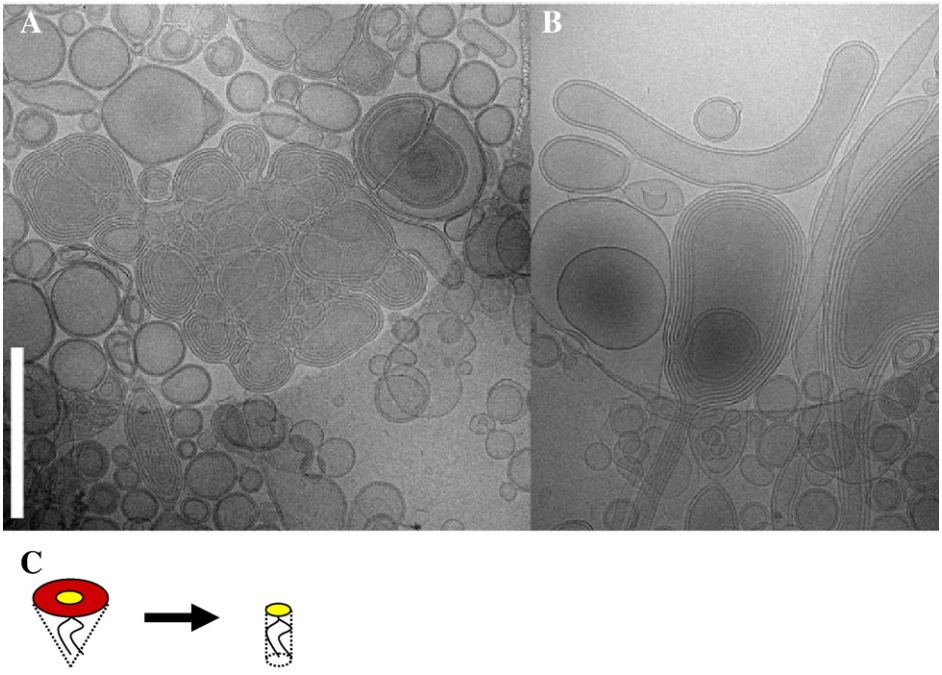

Fig. 9. The effect of buffer at pH = 10 on the BL-forming MVLBG2/DOPC lipid mixture on the nanometer scale. (A, B) Cryo-TEM images of a mixture of MVLBG2 and DOPC (10/90, mol/mol) in buffer at pH = 10. The total lipid concentration is 5 mg/mL. Scale bar, 500 nm. (C) A schematic visualizing the steric (yellow) and electrostatic (red) contributions to size of the MVLBG2 headgroup and thus the lipid's molecular shape. The salt present in the buffer screens the electrostatic contribution (red), while the pH = 10 leads to a deprotonation of the MVLBG2 headgroup, resulting in a reduction of the headgroup charge and size. Consequently, the molecular shape changes from conical to cylindrical, thus favoring zero membrane spontaneous curvature (lamellar structures).

Strong screening of the electrostatic repulsion of the (less highly charged) membranes, as in the high-salt regime, allows formation of multilamellar structures. The intralamellar spacing within the multilamellar structures is again given by the balance between the Van der Waals attraction and combined electrostatic and hydration repulsion.

4. Conclusions

Membrane curvature stabilization is a common phenomenon in cell biology, mainly effected by proteins associated or interacting with membranes. In this work, we have investigated a protein-free system exhibiting membrane curvature stabilization by a highly charged, cone-shaped lipid. The effects of salt and pH, and concomitantly molecular charge and shape, were studied. We have shown that screening of the electrostatic interaction by added salt leads to shape transitions, transforming BLs into other structures. Interestingly, a shape transition from unilamellar to bilamellar vesicles can be seen under low-salt conditions. Further addition of salt results in the formation of multilamellar vesicles. This demonstrates the key role of electrostatic interactions in BL formation. The variation of pH changes the protonation of MVLBG2 and thus the charge and molecular shape of the lipid. However, in our experimental system, the effect of salt – invariably present in buffer systems – dominated. The investigated protein-free membrane model system provides a new approach to understand membrane shape evolution in numerous cellular processes such as endocytosis, endoplasmatic reticulum-associated vesiculation, vesicle recycling, signaling and many others. Considering the results of the present work it is conceivable that the cell could modify the shape of a lipid vesicle by altering the charge or size of lipids or other membrane components.

Acknowledgements

This work was supported by NIH GM-59288, DOE DE-FG-02-06ER46314 and NSF DMR-0803103. Cryo-TEM experiments were conducted at the National Resource for Automated Molecular Microscopy which is supported by the NIH National Center for Research Resources P41 program (RR17573).

References

[1] B. Alberts, Molecular Biology of the Cell4th ed., Garland Science, New York, 2002.
[2] H.T. McMahon, J.L. Gallop, Membrane curvature and mechanisms of dynamic cell membrane remodelling, Nature 438 (2005) 590–596.
[3] R. Parthasarathy, J.T. Groves, Curvature and spatial organization in biological membranes, Soft Matter 3 (2007) 24–33.
[4] J.N. Israelachvili, D.J. Mitchell, B.W. Ninham, Theory of self-assembly of hydrocarbon amphiphiles into micelles and bilayers, J. Chem. Soc., Faraday Trans. 2 (72) (1976) 1525–1568.
[5] J.L. Gallop, P.J.G. Butler, H.T. McMahon, Endophilin and CtBP/BARS are not acyl transferases in endocytosis or Golgi fission, Nature 438 (2005) 675–678.
[6] J.L. Gallop and H.T. McMahon. (2005) in Lipids, Rafts and Traffic, Vol. 72, pp. 223–231.
[7] I.G. Mills, G.J.K. Praefcke, Y. Vallis, B.J. Peter, L.E. Olesen, J.L. Gallop, P.J.G. Butler, P.R. Evans, H.T. McMahon, EpsinR: an AP1/clathrin interacting protein involved in vesicle trafficking, J. Cell Biol. 160 (2003) 213–222.
[8] J.E. Hinshaw, S.L. Schmid, Dynamin self-assembles into rings suggesting a mechanism for coated vesicle budding, Nature 374 (1995) 190–192.
[9] A. Roux, D. Cuvelier, P. Nassoy, J. Prost, P. Bassereau, B. Goud, Role of curvature and phase transition in lipid sorting and fission of membrane tubules, EMBO J. 24 (2005) 1537–1545.
[10] S.Y. Qi, J.T. Groves, A.K. Chakraborty, Synaptic pattern formation during cellular recognition, Proc. Natl. Acad. Sci. U.S.A. 98 (2001) 6548–6553.
[11] A. Zidovska, K.K. Ewert, J. Quispe, B. Carragher, C.S. Potter, C.R. Safinya, Block liposomes from curvature-stabilizing lipids: connected nanotubes, -rods and -spheres, Langmuir 25 (2009) 2979–2985.
[12] K.K. Ewert, H.M. Evans, A. Zidovska, N.F. Bouxsein, A. Ahmad, C.R. Safinya, A columnar phase of dendritic lipid-based cationic liposome–DNA complexes for gene delivery: hexagonally ordered cylindrical micelles embedded in a DNA honeycomb lattice, J. Am. Chem. Soc. 128 (2006) 3998–4006.
[13] J. Quispe, J. Damiano, S.E. Mick, D.P. Nackashi, D. Fellmann, T.G. Ajero, B. Carragher, C.S. Potter, An improved holey carbon film for cryo-electron microscopy, Microsc. Microanal. 13 (2007) 365–371.
[14] C. Suloway, J. Pulokas, D. Fellmann, A. Cheng, F. Guerra, J. Quispe, S. Stagg, C.S. Potter, B. Carragher, Automated molecular microscopy: the new Leginon system, J. Struct. Biol. 151 (2005) 41–60.
[15] J.N. Israelachvili, Intermolecular and Surface Forces2nd ed., Academic Press, London, 1992.
[16] J.H. Lee, V. Agarwal, A. Bose, G.F. Payne, S.R. Raghavan, Transition from unilamellar to bilamellar vesicles induced by an amphiphilic biopolymer, Phys. Rev. Lett. (2006) 96.
[17] J.-Y. Wang, CaseroR.A. , Polyamine Cell Signaling: Physiology, Pharmacology, and Cancer Research1st ed., Humana Press, Totowa, NJ, 2006.
[18] R.J. Bergeron, J.S. McManis, W.R. Weimar, K.M. Schreier, F.L. Gao, Q.H. Wu, J. Ortizocasio, G.R. Luchetta, C. Porter, J.R.T. Vinson, The role of charge in polyamine analog recognition, J. Med. Chem. 38 (1995) 2278–2285.
[19] B.N. Palmer, H. Kipton, J. Powell, Complex-formation between 4,9-diazadodecane-1,12-diamine (spermine) and copper(Ii) ions and protons in aqueous-solution, J. Chem. Soc., Dalton Trans. (1974) 2086–2089.
[20] Y. Takeda, K. Samejima, K. Nagano, M. Watanabe, H. Sugeta, Y. Kyogoku, Determination of protonation sites in thermospermine and in some other polyamines by N-15 and C-13 nuclear magnetic-resonance spectroscopy, Eur. J. Biochem. 130 (1983) 383–389.